Aria of the Dutch North Sea

Sertlek, H.O.; Sertlek H.O.

2.3 SOPRANO HYBRID PROPAGATION MODEL: RANGE-DEPENDENT PROPAGATION EQUATIONS AND RESULTS FOR THE SHALLOW WATER WAVEGUIDES

This section is a modified version of [H.Ö Sertlek, M.A. Ainslie and K.L. Heaney, Range Dependent propagation equations and results for shallow water waveguides, under review by Journal of Acoustical Society of America]

Abstract: *The estimation of propagation loss for a range dependent shallow water waveguide is considered. Specifically, an analytical formulation for the calculation of the depth dependent propagation loss in isovelocity water with a gradually range dependent seabed is introduced. The range dependent bathymetry is handled with Weston's ray invariant approach. The depth dependence of propagation loss is formulated using a transformation from an incoherent mode sum to an integral over angle, in the adiabatic approximation, and the results obtained in this way are tested by comparison with a full adiabatic normal mode sum. The validity of the adiabatic approximation itself is then investigated by means of a comparison with parabolic equation and coupled normal mode results for selected test cases from the Weston Memorial Workshop held at the University of Cambridge in April 2010. The proposed approach provides practical, fast and accurate results.*

2.3.1. INTRODUCTION

The estimation of propagation loss (PL) [Ainslie,2010a; ISO/DIS 18405] for a range dependent shallow water isovelocity waveguide is relevant to various applications of underwater acoustics such as environmental impact assessment, underwater communications and sonar performance modelling. The present section introduces a method that combines the accuracy of an incoherent adiabatic normal mode sum with the speed of Weston's flux integral approach. To solve range dependent propagation problems, normal mode methods apply various approaches such as mode coupling, mode-matching or adiabatic approaches [Jensen et al, 1994]. These approaches are based on a stair-step approximation for the bathymetry and the calculation of normal mode eigenvalues for each stair step. Range dependent normal mode solutions can be computationally expensive for high frequencies or deep water where many modes propagate, and analytical solutions offer a practical alternative that avoids long computational times[Harrison,2005 ; Harrison,2013; Holland,2010]. Weston introduced the flux integral method for evaluation of PL for a variable water depth and arbitrary sound speed profile[Weston,1959]. By using the effective depth approach, Weston [Weston,1976] provided analytical expressions for the depth-averaged propagation factor (*F*) for various depth profiles. An arbitrary bathymetry can be constructed as a combination of these depth profiles. However, the dependence of the propagation factor on receiver and source depths is not visible in this approach.

In the present section, the method of [Weston,1976] is combined with the depth dependent propagation formula of [Sertlek and Ainslie,2013] to derive a formulation for depth-dependent propagation loss in a range dependent waveguide. Discrete and leaky mode effects are also considered, increasing the accuracy of this approach at low frequencies and long ranges. This proposed solution can provide fast and accurate propagation loss predictions for range dependent water depth and sediment type across a wide range of frequencies without summing a large number of normal modes. The results obtained in this way are validated with adiabatic mode theory. Then, the accuracy of the adiabatic mode theory is tested by comparison with coupled mode and parabolic equation model's results. Selected cases from the 2010 Weston Memorial Workshop [Ainslie,2010b] are used, providing insights into the performance of widely used propagation models in a shallow water environment.

This work is motivated by the need for sound mapping across a wide frequency range, namely 10 Hz to 100 kHz, roughly corresponding to the hearing range of marine animals. The proposed

approach enables the calculation of shallow water sound maps in an efficient way without requiring long computation times or advanced computer systems.

2.3.2. DEPTH DEPENDENCE OF PROPAGATION LOSS IN RANGE DEPENDENT WAVEGUIDE

A. Derivation

Propagation loss can be defined in terms of the propagation factor, *F*, as $\mathrm{PL} = 10\log_{10}\frac{F^{-1}}{1\ \mathrm{m}^2}\ \mathrm{dB}$ where F is the propagation factor [Ainslie,2010a; ISO/DIS 18405]. For range independent waveguides, Weston's flux integral can be modified to take into account the depth dependence of the propagation factor [See Section 2.2]. This approach is generalised here for range dependent media. The derivation starts by applying the adiabatic approximation to the incoherent mode sum

$$F(r, z_{\mathrm{r}};\ z_0) = \sum_{n=1}^{\infty} \psi_n^2(z_0, 0)\psi_n^2(z_{\mathrm{r}}, r)R_n^2(r) \tag{1}$$

where the eigenfunction (for isovelocity water) is $\psi_n(z, r) = A_n \sin(\gamma_n(r)z)$ and $R_n(r) = \frac{2\pi}{r\,\kappa_n(r)} \exp\left(-2\int_0^r \delta(r')\mathrm{d}r'\right)$. Here A_n is the amplitude of the *n*th eigenfunction, γ_n is the vertical wavenumber, and κ_n the horizontal wavenumber. The mode decay rate $\delta(r') = -\frac{\ln(|V(\theta_n)|)}{r_{\mathrm{cM}}}$ is the mode attenuation term in the horizontal direction which adds a small imaginary part to κ_n, $r_{\mathrm{cM}} = 2h\cot\theta$ is the modal cycle distance for isovelocity water, and $V(\theta_n)$ is the reflection coefficient of the seabed. The integral in the exponential term for $R_n(r)$ can be written

$$\int_0^r \delta_n(r')\mathrm{d}r' = -D^2(0)\sin^2\theta_0 \int_0^r \frac{\ln(|V(\theta')|)}{2h(r')\cot\theta' D^2(r')\sin^2\theta'}\mathrm{d}r' \tag{2}$$

where

$$D(r) = h(r) + \Delta_{\mathrm{W}} \tag{3}$$

is the wave-shifted water depth, $\Delta_{\mathrm{W}} = \frac{\rho_2/\rho_1}{k_1 \sin\theta_{\mathrm{c}}}$ is the corresponding vertical wave shift[Weston,1994; Weston,1960] and θ_{c} is the critical angle. Eigenvalues for the discrete sum can be approximated using $\gamma_n(r) = \frac{n\pi}{D(r)}$, and $D(0)$ and $D(r)$ are wave-shifted water depths at source and receiver range. Thus, the propagation factor becomes

$$F(r, z_{\mathrm{r}}; z_0) = \frac{2\pi}{r} \sum_{n=1}^{\infty} \frac{\mathrm{A}_{0n}^2 \mathrm{A}_{\mathrm{r}n}^2 \sin^2(\gamma_n(r) z_0) \sin^2(\gamma_n(r) z_{\mathrm{r}})}{k_{\mathrm{r}n}(r)} \exp\left(D^2(0) \sin^2\theta_0 \int_0^r \frac{\ln(|V(\theta')|)}{h(r') D^2(r') \cos\theta' \sin\theta'} \mathrm{d}r' \right) \tag{4}$$

where $A_{0n,rn}^2 = \frac{4}{r_{\mathrm{cM}}(\theta_{0,\mathrm{r}}) \tan\theta_{0.\mathrm{r}}}$. Further, $\theta_{0,\mathrm{r}}$ shows the mode grazing angles at source and receiver ranges and θ'denotes the grazing angle at range r'. Using the trigonometric identity $\sin^2(\gamma_n(r)z) = \frac{1}{2} - \frac{1}{2}\cos(2\gamma_n(r)z)$, and approximating the discrete sum by a continuous angle integral [Sertlek and Ainslie, 2014a] it follows that

$$F_0(r, z_{\mathrm{r}}; z_0) = \frac{2}{r} \int_0^{\theta_{\mathrm{lim}}} \frac{D(0)\cos\theta_0}{h(0) D(r) \cos\theta_{\mathrm{r}}} \left(1 - \mathrm{W}(z_{\mathrm{r}}, z_0, \theta_0)\right) \exp\left(D^2(0) \sin^2\theta_0 \int_0^r \frac{\ln(|\mathrm{V}(\theta')|)}{h(r') D^2(r') \cos\theta' \sin\theta'} \mathrm{d}r' \right) \mathrm{d}\theta_0 \tag{5}$$

where $\theta_{\mathrm{lim}} = \arcsin\left(\frac{\min\{D(0), D(r)\}\sin\theta_{\mathrm{c}}}{D(0)}\right)$. The function $\mathrm{W}(z_{\mathrm{r}}, z_0, \theta_0)$ is

$$\mathrm{W}(z_{\mathrm{r}}, z_0, \theta_0) = \cos(2k_{\mathrm{w}} z_0 \sin\theta_0) + \cos\left(2k_{\mathrm{w}} z_{\mathrm{r}} \frac{D(0)}{D(r)} \sin\theta_0\right) - \frac{\cos(2k_{\mathrm{w}} \zeta_{-} \sin\theta_0) + \cos(2k_{\mathrm{w}} \zeta_{+} \sin\theta_0)}{2} \tag{6}$$

where $\zeta_{\pm} = z_0 \pm z_{\mathrm{r}} \frac{D(0)}{D(r)}$, and Weston's ray invariant relation [Weston,1994]

$$D(r')\sin\theta' = D(0)\sin\theta_0 = D(r)\sin\theta_{\mathrm{r}} \tag{7}$$

is used to relate angles at the source and receiver ranges. Eq.(5) can provide an analytical formulation for range dependent propagation problems. The factor$\left(1 - \mathrm{W}(z_{\mathrm{r}}, z_0, \theta_0)\right)$ results from the product of the source and receiver eigenfunctions. A more detailed physical description of the range independent version of this term and its relation with Weston's solution in [Weston,1980] are provided in Section 2.2.

B. Analytical solution for exponential reflection coefficient

In Eq.(5), different forms for the reflection coefficient can be used. For an exponential reflection coefficient in the form

$$|V_{\mathrm{B}}| = \exp\left(-\eta(r)\frac{\sin(2\theta)}{2}\right) \tag{8}$$

the propagation factor can be written

$$F_0 = \frac{2}{r}\int_0^{\theta_{\mathrm{lim}}} \frac{\mathrm{D}(0)\cos\theta_0}{h(0)D(r)\cos\theta_{\mathrm{r}}}\left(1 - \mathrm{W}(z_{\mathrm{r}}, z_0, \theta_0)\right)\exp\left(-D^2(0)\sin^2\theta_0 \int_0^r \frac{\eta(r)}{h(r')D^2(r')}\mathrm{d}r'\right)\mathrm{d}\theta_{\mathrm{s}} \tag{9}$$

This integral gives the propagation factor for range dependent media. If one ignores the wave and beam [Sertlek and Ainslie, 2014a;Weston,1994] shifts for high-order modes and assumes $\cos\theta_{0,\mathrm{r}} \approx 1$ (consistent with the small angle approximation), it follows that

$$F_0 = \frac{2}{rh(r)} \int_0^{\theta_{\lim}} \left(1 - \mathrm{W}(z_r, z_0, \theta_0)\right) \exp\left(-h^2(0)\, {\theta_0}^2 \langle \frac{\eta}{h^3} \rangle r\right) \mathrm{d}\theta_0 \qquad (10)$$

where $\langle \frac{\eta}{h^3} \rangle$ is the average value of $\frac{\eta}{h^3}$ from the source (at range zero) to range r. In Appendix A this quantity is evaluated analytically using Weston's effective depth approach [Weston,1976]. Eq.(10) can be solved analytically in the terms of Faddeeva functions as described by SA-25 (using SA-*n* here and throughout to denote Eq. (*n*) from Section 2.2.). In this way, the analytical solution for Eq.(10) can be obtained as

$$\begin{aligned} & F_0(r, z_r; z_0) \\ & = r^{-\frac{3}{2}} \sqrt{\frac{\pi}{\eta h_{\mathrm{eff}}}}\, \mathrm{erf}\left(\sqrt{h^2(0) \langle \frac{\eta}{h^3} \rangle r}\, \theta_{\lim}\right) \\ & - \left\{ \frac{2}{rh_r} \left[\boldsymbol{\Phi}\left[2k_w z_0, h^2(0) \langle \frac{\eta}{h^3} \rangle r, \theta_{\lim}\right] + \boldsymbol{\Phi}\left[2\frac{D(0)}{D(r)} k_w z_r, h^2(0) \langle \frac{\eta}{h^3} \rangle r, \theta_{\lim}\right] \right.\right. \\ & \left.\left. - \frac{\boldsymbol{\Phi}\left[2k_w \zeta_-, h^2(0) \langle \frac{\eta}{h^3} \rangle r, \theta_{\lim}\right] + \boldsymbol{\Phi}\left[2k_w \zeta_+, h^2(0) \langle \frac{\eta}{h^3} \rangle r, \theta_{\lim}\right]}{2} \right] \right\} \end{aligned} \qquad (11)$$

where

$$\begin{aligned} \Phi[Z, R, \theta_{\lim}] &= \int_0^{\theta_{\lim}} \cos(Z\theta) \exp(-R\,\theta^2) \mathrm{d}\theta \\ &= \sqrt{\frac{\pi}{R}} \frac{\exp\left(-\frac{Z^2}{4R}\right)}{4} \left[\mathrm{w}\left(\frac{Z}{2\sqrt{R}} - \mathrm{i}\sqrt{R}\theta_{\lim}\right) \exp\left(\left(\frac{Z}{2\sqrt{R}} - \mathrm{i}\sqrt{R}\theta_{\lim}\right)^2\right) \right. \\ &\quad \left. - \mathrm{w}\left(\frac{Z}{2\sqrt{R}} + \mathrm{i}\sqrt{R}\theta_{\lim}\right) \exp\left(\left(\frac{Z}{2\sqrt{R}} + \mathrm{i}\sqrt{R}\theta_{\lim}\right)^2\right) \right] \end{aligned} \qquad (12)$$

and $\mathrm{w}(x+\mathrm{i}y)$ is the Faddeeva function[Abramowitz and Stegun,1972]. For the large *R* limit $\left(\frac{Z}{2\sqrt{R}} \ll \sqrt{R}\,\theta_{\mathrm{lim}}\right)$, $\mathbf{\Phi}[Z,R,\theta_{\mathrm{c}}] \approx \frac{1}{2}\sqrt{\frac{\pi}{R}}\exp\left(-\frac{Z^2}{4R}\right)$ and $\mathrm{erf}\left(\sqrt{h^2(0)\,\langle\frac{\eta}{h^3}\rangle\,r}\,\theta_{\mathrm{lim}}\right) \approx 1$. In this limit, the solution simplifies to

$$F_0(r,z_{\mathrm{r}};\,z_0) = r^{-\frac{3}{2}}\sqrt{\frac{\pi}{\eta h_{\mathrm{eff}}}}\left(1-\exp(-2\phi_0^2k_{\mathrm{w}}^2z_0^2)-\exp\left(-2\phi_0^2k_{\mathrm{w}}^2z_{\mathrm{r}}^2\frac{D^2(0)}{D^2(r)}\right)\right.$$
$$\left.+\frac{\exp(-2\phi_0^2k_{\mathrm{w}}^2(\zeta_-)^2)+\exp(-2\phi_0^2k_{\mathrm{w}}^2(\zeta_+)^2)}{2}\right) \qquad (13)$$

where $\phi_0 = \sqrt{\frac{1}{2\,h^2(0)\,H_\eta}}$, $\langle\frac{\eta}{h^3}\rangle = \frac{\eta h_{\mathrm{eff}}}{h^2(0)h^2(r)}$ for a constant η, and Eq.(13) is a generalisation of SA-37 to the range dependent situation (SA-37 is identical to Eq (9) of [Weston,1991], which was not cited by [Sertlek and Ainslie,2014a] because they were unaware of the existence of [Weston,1991] at that time). Equation (13) is valid for constant η and in the limit of large *R*.

2.3.3. DISCRETE MODE EFFECTS FOR RANGE DEPENDENT MEDIA

At short ranges, where many modes are present, the discrete mode sum may be approximated by an integral over a continuum of modes [Harrison and Ainslie,2010]. In the mode stripping region, the number of modes that contribute to the sound pressure field decreases with increasing range, until at some point there remains only a handful, so that the integral ceases to provide a good approximation to the discrete sum. This point is the end of the mode stripping region and the beginning of a region in which the discreteness of the mode sum becomes important [Ainslie,2010a]. In order to retain accuracy in this discrete mode region, a few low-order modes can be separated from the integral solution. In other words

$$F = \underbrace{\sum_{n=1}^{M}\psi_n^2(z_0)\psi_n^2(z_{\mathrm{r}},r)R_n^2(r)}_{F_M} + \underbrace{\sum_{n=M+1}^{\infty}\psi_n^2(z_0)\psi_n^2(z_{\mathrm{r}},r)R_n^2(r)}_{G_M} \qquad (14)$$

Replacing G_M by an integral approximation for a continuum of modes, and applying the symmetry property identified by SA-30, we obtain

$$G_M(z_\mathrm{r}, z_0) = \begin{cases} F_-(z_\mathrm{r}, z_0), z_0 < D/2 \\ F_+(z_\mathrm{r}, z_0), z_0 > D/2 \end{cases} \quad (15)$$

where $F_- = \begin{cases} G_{M0}(z_\mathrm{r}, z_0) & , z_\mathrm{r} < D/2 \\ G_{M0}(D - z_\mathrm{r}, z_0), & z_\mathrm{r} > D/2 \end{cases}$ and $F_+ = \begin{cases} G_{M0}(z_\mathrm{r}, D - z_0) & , z_\mathrm{r} < D/2 \\ G_{M0}(D - z_\mathrm{r}, D - z_0), & z_\mathrm{r} > D/2 \end{cases}$.

G_{M0} is the continuous angle representation of the propagation factor

$$\mathrm{G_{M0}} = \frac{2}{r}\int_{\theta_{M+1/2}}^{\theta_\mathrm{lim}} \frac{D(0)\cos\theta_0}{h(0)D(r)\cos\theta_\mathrm{r}}\left(1 - \mathrm{W}(z_\mathrm{r}, z_0, \theta_0)\right)\exp\left(\left(D^2(0)\sin^2\theta_0 \int_0^r \frac{\ln(|V(\theta')|)}{h(r')D^2(r')cos\theta' \sin\theta'}\mathrm{d}r'\right)\right)\mathrm{d}\theta_0 \quad (16)$$

The lower integration limit is $\theta_{M+1/2} \equiv \frac{\theta_M + \theta_{M+1}}{2}$ because the first M modes are summed separately. Eq.(15) helps to obtain the properties at the sea surface (or seabed) and source (or complementary source) depths. The mode attenuation is calculated with the Kornhauser and Raney approximation [Kornhauser and Raney,1955] and adiabatic approach. The resulting modal decay rate[Ainslie et al,1993] is

$$\beta_n(r') = \frac{\epsilon\gamma_n^2(\rho_\mathrm{sed}/\rho_\mathrm{w})\cot^3\theta_\mathrm{c}\sec\theta_\mathrm{c}}{hk_\mathrm{w}\sqrt{k_\mathrm{w}^2 - \gamma_n^2}\left(\left(1 - \frac{\gamma_n^2}{k_\mathrm{w}^2\sin^2\theta_c}\right)^{1/2} + \frac{\rho_\mathrm{sed}^2\gamma_n^2}{\rho_\mathrm{w}^2 k_\mathrm{w}^2\sin^2\theta_\mathrm{c}} + \frac{\rho_\mathrm{sed}}{\rho_\mathrm{w}k_\mathrm{w}h\sin\theta_\mathrm{c}}\right)} \quad (17)$$

where ρ_sed and ρ_w are the densities of seawater and sediment, respectively, and ϵ is the fractional imaginary part of the sediment wavenumber. This equation was derived from mode theory formulas that implicitly take into account wave and beam shifts [Weston,1994]. In Eq. (17) we choose not to neglect such wave and beam shifts because the presence of these terms in the exponent leads to important corrections that are needed to maintain accuracy at long range. The contribution to the propagation factor from the first *M* discrete modes can be written as

$$F_M = \frac{8\pi}{rD(0)D(r)} \sum_{n=1}^{M} \frac{\sin^2(\gamma_n z_0)\sin^2(\gamma_n z_r)}{\sqrt{k_w^2 - \gamma_n^2}} \exp\left(-2\int_0^r \beta(r')\mathrm{d}r'\right) \qquad (18)$$

Finally, the hybrid formulation of the propagation factor in range dependent media can be written analytically by ignoring the wave shifts for high-order of modes and using the small angle approximation (by assuming $\cos\theta_{0,r} \approx 1$),

$$F = F_M + \frac{2}{rh(r)} \int_{\theta_{M+1/2}}^{\pi/2} \left(1 - W(z_r, z_0, \theta_0)\right) \exp\left(\left(h^2(0)\sin^2\theta_0 \int_0^r \frac{\ln(|V(\theta)|)}{h^3(r')\sin\theta}\mathrm{d}r'\right)\right)\mathrm{d}\theta_0 \qquad (19)$$

Any form for the reflection coefficient, including both exact or approximate forms of the Rayleigh refection coefficient [Harrison,2010] can be used for $V(\theta)$, depending on the desired accuracy. Use of the exact form in the numerical solutions increases accuracy and permits calculations above the critical angle [Harrison,2010], by extending the upper integration limit to $\frac{\pi}{2}$, thus taking into account the contribution from leaky modes. Including leaky mode terms in the integrand of the adiabatic approach (exponential term in Eq.(18)) provides a smoother transition in the upslope region in the examples that follow, in which ray paths are continually steepened, and the corresponding modes pass from the discrete spectrum to the continuous spectrum. In the downslope region after the ridge, the same effect happens in reverse, with the discrete mode spectrum continually re-populated by a process of downslope conversion.

2.3.4. COMPARISONS

A. Comparison Procedure:

Description of Test Cases

In these comparisons, test cases derived from Scenarios A2.I and A2.IV from the Weston Memorial Workshop (WMW) are used [Zampolli et al,2010]. The purpose of the WMW, held at the University of Cambridge in April 2010[Ainslie,2010b], was to improve understanding of signal to noise ratio and signal to reverberation ratio for simple sonar performance problems based on the 2006 ONR workshop[Thorsos and Perkins,2007]. Following [Sertlek and Ainslie,2013] and [Ainslie et al,2013], the selected test cases are referred to as "Case 1", "Case 4" and "Case 9". Cases 1 and 4 are identical to Scenarios A2.I and A2.IV, respectively, except that absorption in water and seabed roughness are both set to zero. Case 9 is a modified form of Case 4 suggested by Preston[Preston and Ellis,2012; Ellis and Pecknold,2012]. In all comparisons, the source depth (z_{s}) is $30\ \mathrm{m}$, sound speed in water (c_{w}) and sediment (c_{s}) are, respectively, $1500\ \mathrm{m/s}$ and $1700\ \mathrm{m/s}$. The sediment-seawater density ratio is 2 and the sediment absorption coefficient (β), in units of decibels per wavelength, is 0.5, corresponding to an absorption coefficient per unit frequency of 0.294118 dB/(m kHz). (The sediment absorption coefficient is related to fractional imaginary part of complex sediment wavenumber by means of $\epsilon = \beta \ln(10)/40\pi$). The comparisons start with the range independent case (Case 1), which has 100 m water depth. More detailed comparisons were done for this range-independent case in [Section 2.2]. Case 4 has 100 m water depth up to 5 km from the source. Then, it features an upslope region from 5 km to 7 km up to water depth 30 m, with uniform water depth thereafter. Case 9 follows Case 4 to 8 km. The shallow water region (depth 30 m) is then followed by a downslope region from 8 km to 10 km down to water depth 100 m, and uniform depth thereafter (Fig. 1). Case 9 is identical to Case 4 in all respects other than these differences in bathymetry.

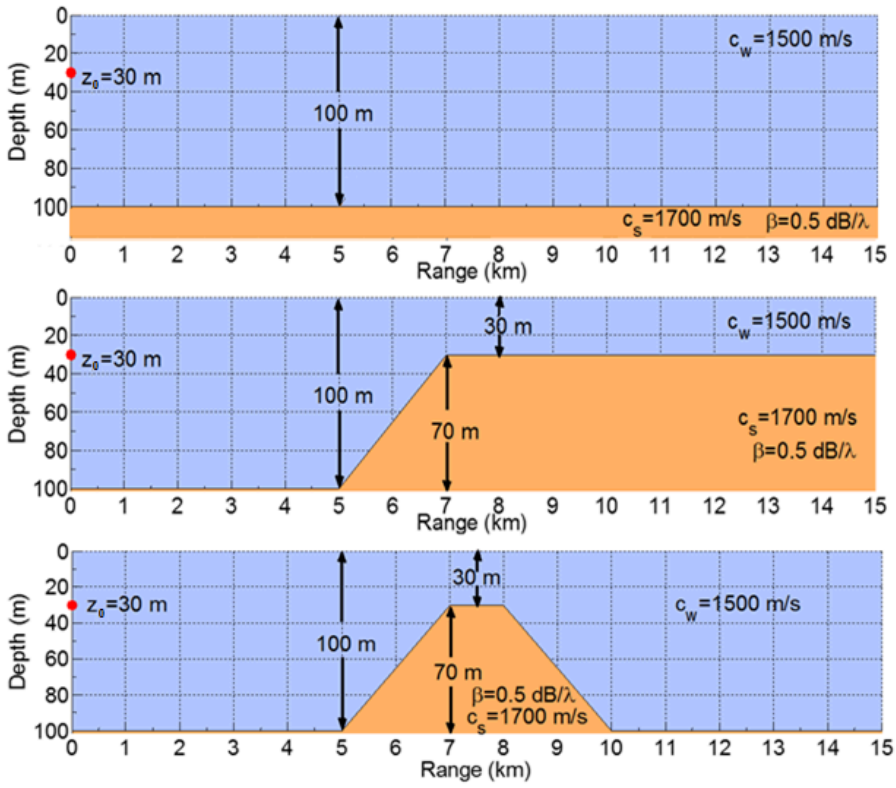

Figure 1. The bathymetry of Cases 1,4 and 9

Comparisons are made for the frequencies 250 Hz, 1 kHz and 3.5 kHz. For normal mode solutions, KrakenC and Couple are used. KrakenC is a normal mode algorithm that can handle range dependent problems with adiabatic and coupled mode approaches [Porter,1990]. For KrakenC's solution, we select the incoherent adiabatic option, which is based on complex eigenvalues and a stair-step approximation of the bathymetry. Couple is also a normal mode program, developed for obtaining normal mode solutions with various coupled mode approaches [Evans,1983]. Couple's solution (a coherent mode sum) is also based on a stair-step approximation. The proposed equations ((Eq.(11) ,Eq.(13) and Eq.(19))) in this section (incoherent mode sums) are based on a piecewise-linear bathymetry. For range dependent solutions, Δr_n equals 10 m as a stair-step length (in the mode theory solution) and piecewise-linear segment size (in the proposed integral solution) to have comparisons with the same resolution. Peregrine[Heaney and Campbell,2015] is an in-house version of RAM[Collins,1993] for parabolic equation calculations.

Reference and Relative PL

The challenge addressed here is that of magnifying small differences in PL predictions, when the individual PL curves exhibit a large dynamic range. In this situation, the use of a reference propagation loss curve and plotting the relative propagation loss as

$$\mathrm{PL}_{\mathrm{relative}}(r) = \mathrm{PL}(r) - \mathrm{PL}_{\mathrm{ref}}(r) \tag{20}$$

can help to zoom in on detailed features. If the reference $\mathrm{PL}_{\mathrm{ref}}(r)$ is chosen to describe the general PL trend, $\mathrm{PL}_{\mathrm{relative}}$ then describes the departure from that trend. In the following, Weston's flux integral[Weston,1976] is chosen as the reference propagation factor

$$F_{\mathrm{ref}} = \frac{2}{rh(r)}\int_0^{\theta_{\mathrm{lim}}} \exp\left(-\frac{{\theta_{\mathrm{s}}}^2\, h_{\mathrm{eff}}}{h^2(r)}r\right)\mathrm{d}\theta_{\mathrm{s}} = r^{-\frac{3}{2}}\sqrt{\frac{\pi}{\eta h_{\mathrm{eff}}}}\,\mathrm{erf}\left(\sqrt{\frac{\eta r h_{\mathrm{eff}}}{h^2(r)}}\theta_{\mathrm{lim}}\right) \tag{21}$$

such that the reference propagation loss is $\mathrm{PL}_{\mathrm{ref}} = 10\log_{10}\frac{F_{\mathrm{ref}}^{-1}}{1\ \mathrm{m}^2}$ dB. The value chosen for the reflection loss gradient (η) is 0.273777 Np/rad [from page 454 of Ref.1], and the effective water depth is $h_{\mathrm{eff}} = \frac{h^2(0)h^2(r)}{r}\int_0^r \frac{1}{h(r')^3}\mathrm{d}r'$, which is evaluated analytically by using piecewise linear approximation for the bathymetry, as described in the Appendix. Equation (21) also follows from Eq.(9) for a uniform sediment type and with $\mathrm{W}(z_{\mathrm{r}}, z_{\mathrm{s}}, \theta_{\mathrm{s}}) = 0$. In Fig. 2, $\mathrm{PL}_{\mathrm{ref}}$ versus range is shown for Cases 4 and 9. The $\mathrm{PL}_{\mathrm{relative}}$ curves plotted in subsequent graphs quantify the departures from the corresponding curves in Fig 2.

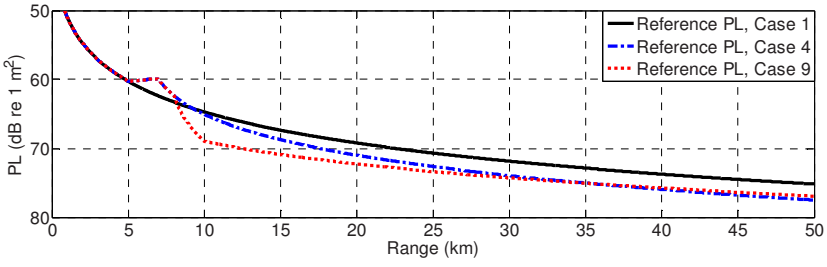

Figure 2. Reference PL for the test cases (Eq. 21 is used)

B. Validations: Comparisons with adibatic mode theory

Leaky mode contributions

Eq. (19) and KrakenC results can be evaluated with or without the leaky mode contribution. In order to include the contribution from leaky modes, the continuum integral in Eq.(19) is extended to $\pi/2$, thus taking into account the eigenvalues whose grazing angles are beyond the critical angle. The contribution from leaky modes to the depth-averaged PL is shown in Fig. 3 for Cases 1, 4 and 9 at 250 Hz. All three are identical up to 5 km, after which the influence of the upslope region can be seen for Cases 4 and 9. First, Fig. 3 shows the effect of leaky (supercritical) modes on relative PL at short range (up to 2 km) Most of the initially generated leaky modes lose their energy within a few kilometres of the source, thus explaining the rapid initial decay of the leaky mode contributions in Fig.3, especially during the first kilometre. The range-dependent test cases (4 and 9) are identical up to 8 km. In these, ray paths are steepened by the upslope propagation between 5 km and 7 km, resulting in the conversion of discrete (trapped) modes into leaky ones that then decay quickly at the top of the slope, from 7k m to 8 km. Beyond 8 km, the curves for Cases 4 and 9 differ because of the different bathymetry, but no new leaky modes are generated beyond this point. This figure also shows the agreement between KrakenC and Eq.(19) with and without leaky mode contribution.

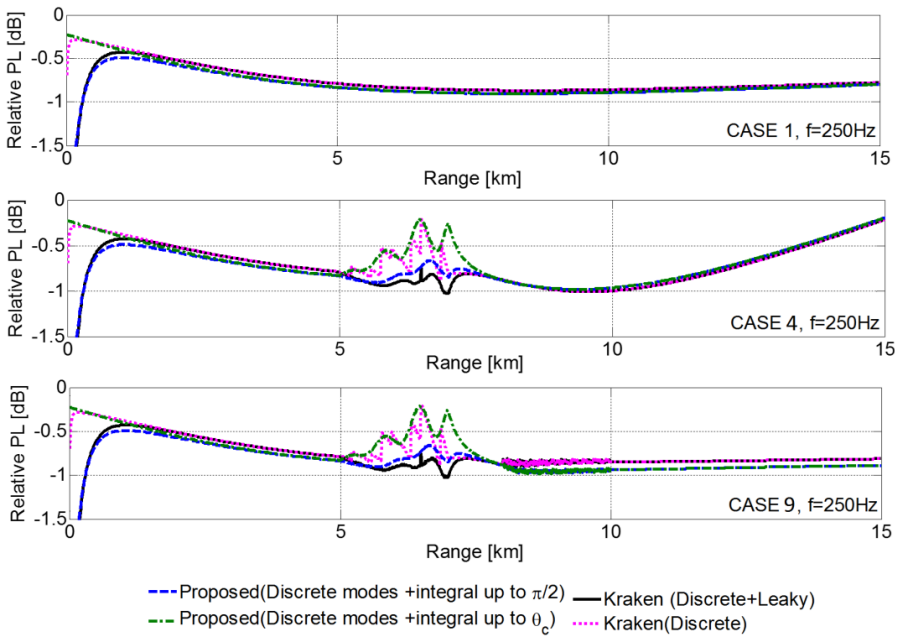

Figure 3. Eq.(19) is integrated up to critical angle and $\pi/2$ (with 5 discrete modes) to exclude and include leaky modes. Solutions of Eq.19 are compared with KrakenC without (with) leaky mode contribution. The exact Rayleigh reflection coefficient is used for the seabed reflection coefficient in Eq.(19).

Up to 500 m, the contribution of the leaky modes exceeds 1.2 dB. Then, the leaky mode contribution becomes less than 0.01 dB between 2 km and 5 km. The contribution from leaky modes is about 0.6 dB between 5 km and 8 km for the depth averaged PL, and is negligible at all other distances beyond 1 km. The proposed method agrees with the KrakenC adiabatic mode sum to within 0.2 dB when the upper limit of the angle integral is extended to $\frac{\pi}{2}$. Eq.(19) can be implemented easily and generates a fast solution without requiring the estimation of eigenvalues, which is computationally expensive, especially for high frequencies.

Validations for the relative PL field

In this section, the relative PL field (i.e., PL relative to $\mathrm{PL}_{\mathrm{ref}}$) is investigated. Results for Cases 4 and 9 are shown in Figs. 4 and 5, calculated using Eq.(19) and Eq.(13). The solutions based on Eq.(19) (left hand graphs), which include the contribution from leaky modes, replicate the

adiabatic form of KrakenC's results (not shown). The contribution from leaky modes can be significant over the slopes (as shown in Fig.4), and at low frequency Eq. (13) fails to capture the discrete nature of the mode sum. The solutions based on Eq.(13) (right hand graphs) use the exponential reflection coefficient and asymptotic form of $\Phi[Z, R, \theta_{\lim}]$ for large R, which is described by Eq.(12).

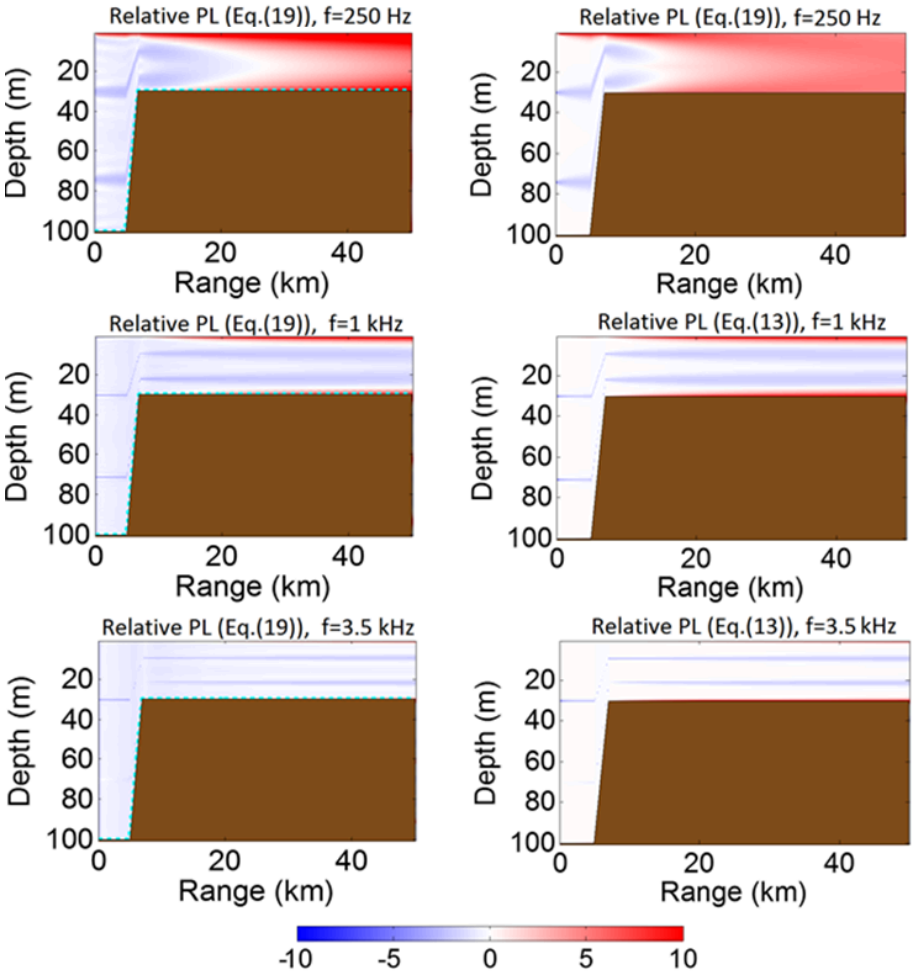

Figure 4. the relative propagation loss $PL - PL_{\text{ref}}$ [dB] field for Case 4 at 250 Hz,1 kHz and 3.5 kHz using Eq.(19) (left) and Eq.(13) (right). Eq.(19) is evaluated using the exact Rayleigh reflection coefficient for M = 5, and including leaky modes; Eq.(13) is an approximate continuous integral solution and excludes leaky modes. The source depth is 30 m.

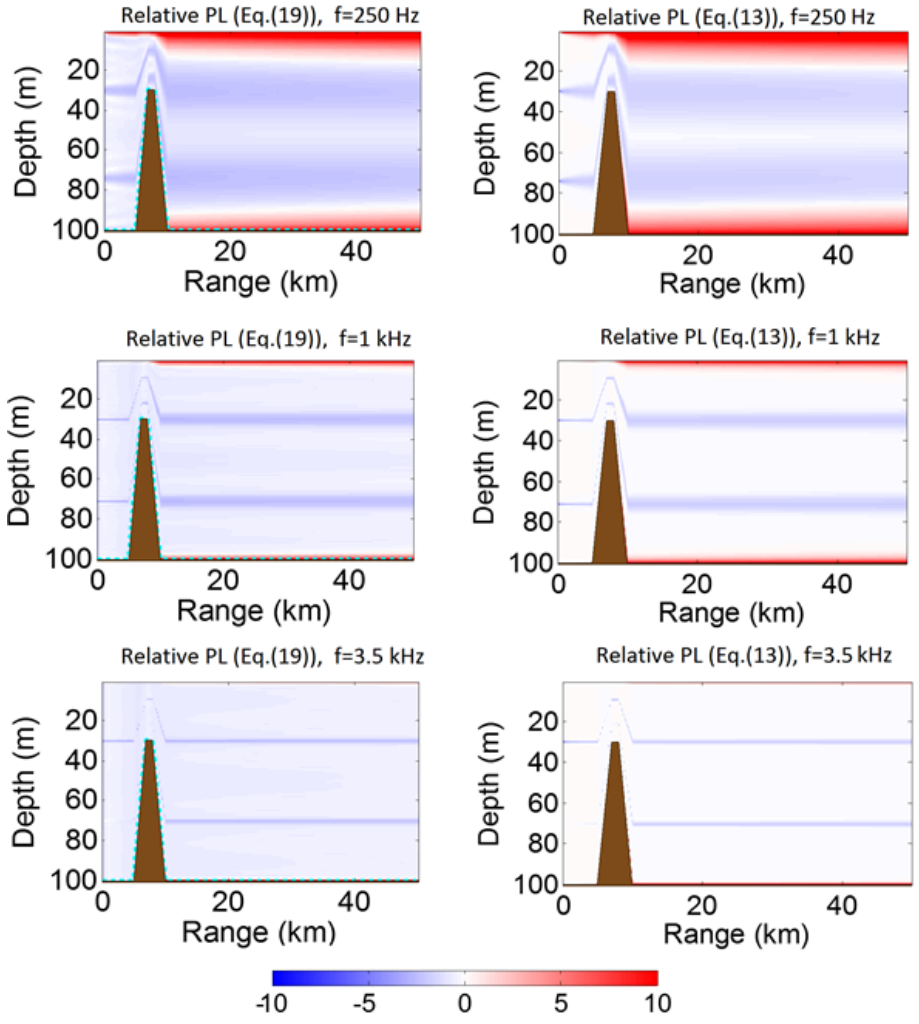

Figure 5. The relative propagation loss $PL - PL_{\mathrm{ref}}$ [dB] field for Case 9 at 250 Hz,1 kHz and 3.5 kHz using Eq.(19) (left) and Eq.(13) (right). Eq.(19) is evaluated by the exact Rayleigh reflection coefficient for M = 5, and including leaky modes; Eq.(13) is an approximate continuous integral solution and excludes leaky modes. The source depth is 30 m.

Wave theory features of two kinds are visible in these graphs: near the boundaries, surface decoupling effects cause the reference PL function, given by Weston's original flux integral (Eq.(21)) underestimates the propagation loss, and this region appears in red; and at the source and complementary depths there exist coherent enhancenments [Weston,1980] that appear as

parallel blue streaks. In the adiabatic approximation, these streaks follow the slopes in the bathymetry. Considering its simplicity, Eq.(13) provides a surprisingly accurate analytical formulation for PL, especially for long ranges.

Comparisons between Proposed Approach and incoherent mode sum: PL_{Relative} vs depth

In Fig.6, PL vs depth comparisons are shown. Cases 4 and 9 have the same bathymetry up to 8 km from the source. Thus, the first and second comparisons are valid for both cases. The third comparison is for Case 4. The last comparison is for Case 9.

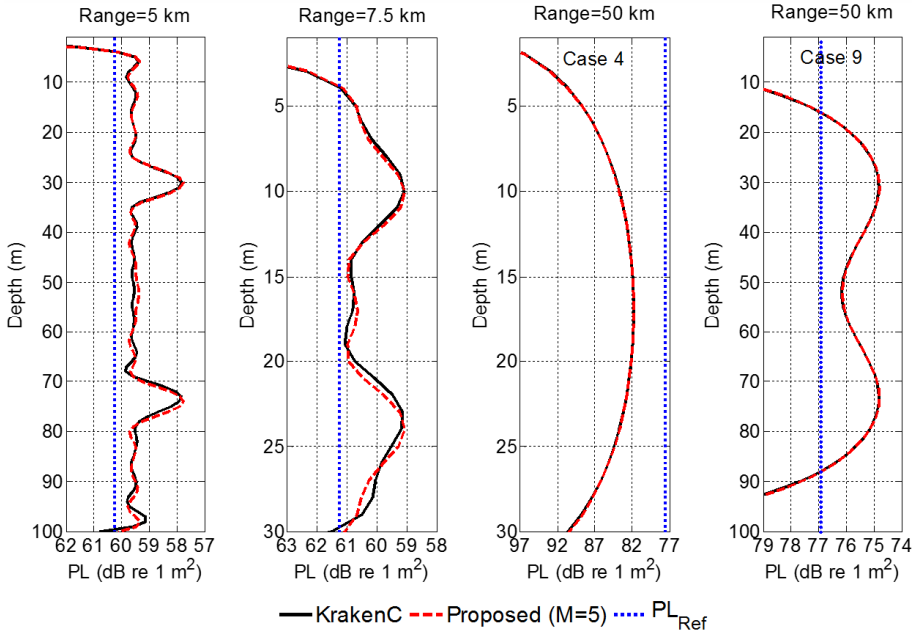

Figure 6. Relative PL vs depth comparisons with discrete mode region effects (M=5, no leaky modes) for 250 Hz at 5 km, 7.5 km and 45 km. The Rayleigh reflection coefficient is used for Eq.(19).The source depth is 30 m. The bathymetries for Cases 4 and 9 are the same until 8 km. Thus, the first depth vs PL graph is the same for Cases 1, 4 and 9; similarly, the first two depth vs PL graphs are the same for Cases 4 and 9; The third graph (note the different y axis scale) is for Case 4. The last one is for Case 9, The reference solution is evaluated using Eq.(21).

Good agreement is obtained between Eq.(19) and KrakenC (adiabatic) for the depth dependent propagation loss. At low frequencies for which only a few modes propagate, the mode region effects must be considered when estimating PL especially at long ranges. Eq.(19) can provide a solution as accurate as that of KrakenC(Adiabatic), without requiring complex root finding algorithms.

Comparisons for different number of discrete modes

In principle, the accuracy of Eq.(19) at long range and low frequency can be improved by adding more modes, and eventually one can expect the result to converge. In practice it converges for a surprisingly small number of discrete modes, as shown below. In Fig, 7, the relative PL for Case 4 is shown for different numbers of mode contributions at three frequencies.

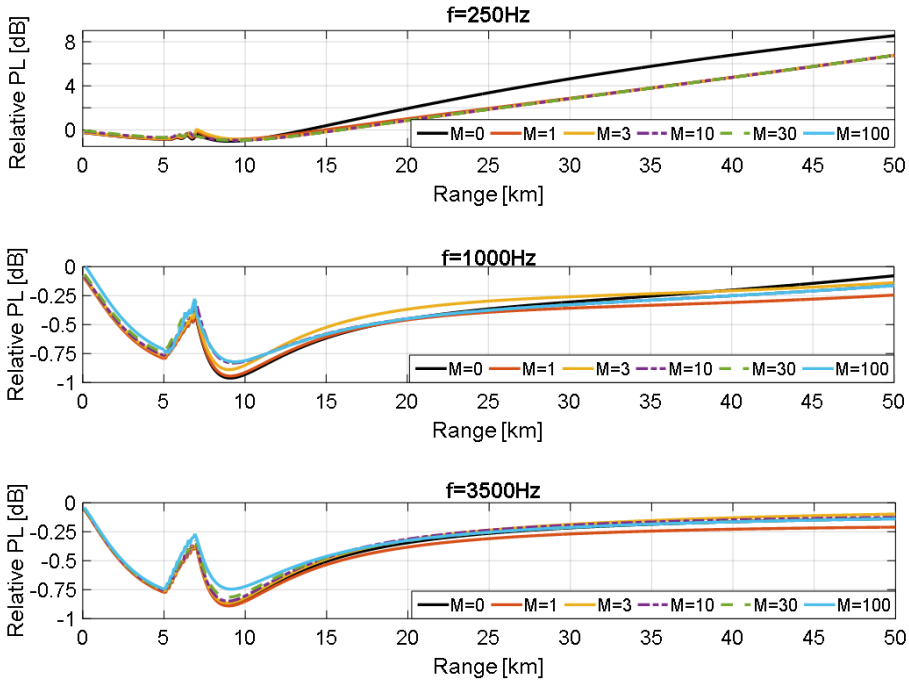

Figure 7. The effect of the number of discrete modes on the convergence of propagation loss. The mode sum incudes only discrete modes, thus excluding paths steeper than the critical angle. The range step size is chosen to be 100 m for these comparisons. Note the different y axis scale at 250 Hz.

Convergence tests can provide insight into how many modes (M) can be enough. This therefore demonstrates that using M = 3 provides sufficient accuracy to provide a mode solution at low frequencies and long ranges (compared with M = 5 actually used). For low frequencies, the contribution from the integral part decreases. For high frequencies, such that many modes propagate, the continuum approach is more efficient than a discrete sum. Thus, adding more modes at high frequencies (1 and 3.5 kHz) does not make a significant contribution. Adding even only one mode at low frequency (250 Hz) helps convergence.

Comparisons for the computation time

In Fig 8, the running times of KrakenC and Eq.(19) are compared for Cases 1 and 9. For Case 9, the PL is calculated at every 50 m up to 45 km for frequencies between 30 Hz to 10 kHz. The adiabatic mode sum option is used in KrakenC. This comparison shows that similar accuracy with adiabatic mode theory can be obtained without requiring long calculation times. Eq.(19) is more than 1000 times faster than KrakenC at 10 kHz for Case 9 because it does not require any numerical algorithms for the estimation of eigenvalues. For the range indepedent case, which only requires the calculation of one set of eigenvalues by KrakenC, Eq.(19) is still more than 100 times faster than KrakenC at frequencies above 3 kHz.

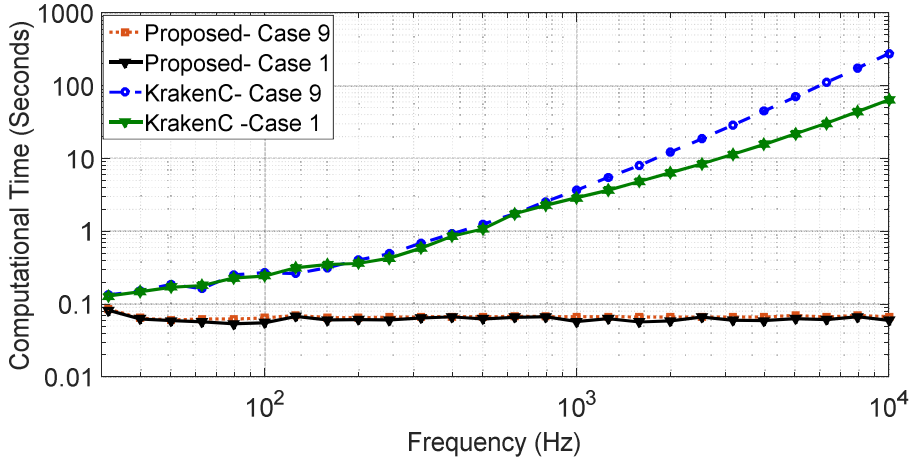

Figure 8. The computation times for KrakenC and Eq.(19) ("Proposed"). The stair-step size is 50 m for KrakenC.

C. Multiple Model Comparisons for Depth Averaged PL

In this section, depth-averaged $\mathrm{PL}_{\mathrm{relative}}$ vs range results (obtained by averaging mean-square sound pressure over receiver depth between the sea surface and seabed) are compared for Cases 1, 4 and 9, with the purpose of quantifying the accuracy of the solutions from different models. To achieve this we first establish a "baseline" solution that is trusted withing a specified tolerance. Specifically, a baseline for the depth-averaged propagation loss is established when the maximum difference of the solutions predicted by Peregrine and Couple, for Cases 4 and 9, is less than 0.5 dB. For Case 1, the same criterion applies except that KrakenC replaces Couple for this range-independent environment. The baseline is equal to the average in decibels of the two (equivalent to taking the geometric mean of the depth-averaged propagation factors) at each range. These two models are chosen because they rely on different approaches for solving the Helmholtz equation[Jensen et al, 1994], one applying a marching solution with the paraxial approximation[Collins,1993] and the other applying a discrete normal mode expansion, including leaky modes. Because of the radically different nature of the nature of the approximations made, if, for any specific test case, these different approaches result in essentially the same solution, we consider it reasonable to infer from this agreement that the errors are small for both models. While this approach falls short of providing proof of accuracy (see, e.g.[Collins and Evans,1992] and [Porter et al,1991] for counter-examples), it provides a strong indication that errors are small, and we argue, in the sense of Reference 3 that the burden of proof is on others to identify and correct any errors in the baseline solution. In the following paragraphs, we investigate the difference between the baseline solution and the adiabatic approximation for Cases 4 and 9. In Table 1, the differences between Peregrine and Couple solutions are shown, providing a measure of the uncertainty in the baseline solutions. The 0.5 dB criterion for establishing a baseline is met for all combinations except for Case 4 at 3.5 kHz. Cases 1, 4 and 9 are now considered in turn.

Table 1. Maximum difference between Peregrine and normal mode (Couple or Kraken) solutions (magnitude of difference, in dB). A baseline is established for all combinations except Case 4 at 3.5 kHz, for which the maximum error exceeds 0.5 dB.

	250 Hz	**1 kHz**	**3.5 kHz**
Case 1 (Peregrine cf KrakenC)	0.1 dB	0.1 dB	0.1 dB
Case 4 (Peregrine cf Couple)	0.2 dB	0.1 dB	0.7 dB
Case 9 (Peregrine cf Couple)	0.2 dB	0.2 dB	0.3 dB

For Case 1 (Fig 9), at short range, Eq.(19) agrees with the baseline solution because of taking into account leaky mode effects. At long range, the differences between Eq.(19) and the baseline solution less than 0.15 dB for all three frequencies.

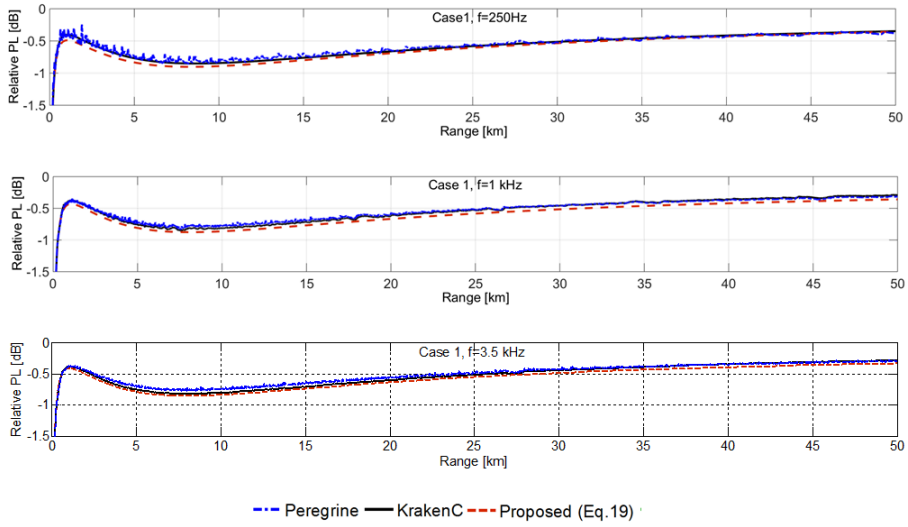

Figure 9. Comparisons for Case 1. Relative PL ($PL\ (depth\ averaged) - PL_{ref}$) results of KrakenC, Peregrine and Eq.(19). The exact Rayleigh reflection coefficient is used for Eq.(19). The source depth is 30 m. The squared sound pressure is averaged over receiver depths with 1 m resolution.

Results for Case 4 (Fig 10) and Case 9 (Fig 11) are identical to Case 1 up to 5 km and are not shown. For 250 Hz, the adiabatic approximation (KrakenC and Eq. (19)) replicate the baseline solution within 0.15 dB between 5 km and 10 km. At longer range, the adiabatic approximation overestimates the depth-averaged PL by up to 0.35 dB.

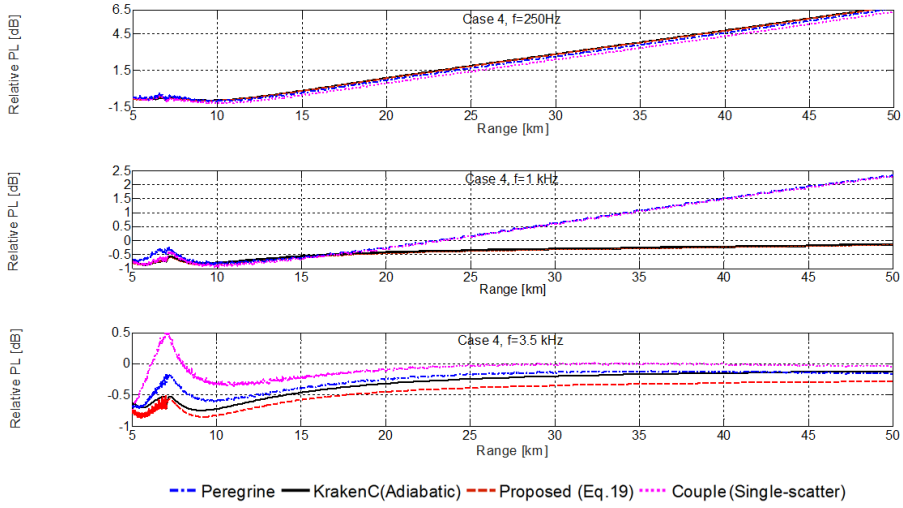

Figure 10. Comparisons for Case 4. Relative PL ($PL\ (depth\ averaged) - PL_{ref}$) results of KrakenC-Adiabatic(incoherent), Couple(Coherent), Peregrine(coherent) and Eq.(19)(incoherent). Exact Rayleigh Reflection coefficient is used for Eq.(19). The source depth is 30 m. The squared sound pressure is averaged over receiver depths with 1 m resolution. Note the different y axis scales for these comparisons.

For 1 kHz, the adiabatic approximation underestimates PL by an amount that increases with increasing range beyond 17 km. The difference between KrakenC and the baseline solution becomes 2.3 dB at 50 km.These comparisons show that the adiabatic approximation can replicate Peregrine solutions for 250 Hz and 3.5 kHz. At 250 Hz there is only one mode in the shallow water part, which is travelling at a steep angle, so there is no reason to expect a problem with the adiabatic approximation. Specifically, the steep ray path ensures a short cycle distance, and hence small changes in water depth for each ray cycle. At 1 kHz there is a region in which there is only one mode left, and this mode is not steep. In turn this implies a long cycle distance, and the potential for large changes in water depth per ray cycle in the sloping regions. This probably

causes the larger difference between adiabatic approximation and baseline solution at this frequency.

For Case 9 (Fig 11), the differences between KrakenC and the baseline solution are less than 0.6 dB for 250 Hz, 0.2 dB for 1 kHz and 0.4 dB for 3.5 kHz.

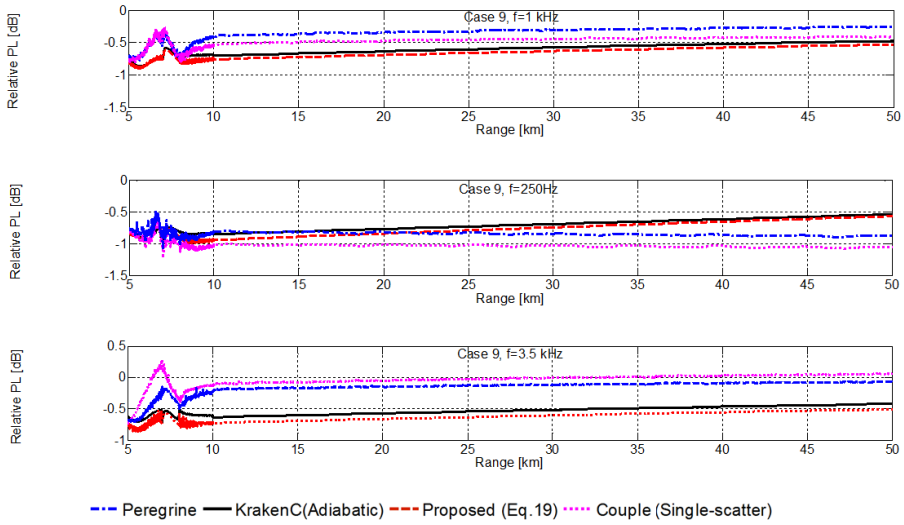

Figure 11 . Comparisons for CASE 9. Relative PL ($PL\ (depth\ averaged) - PL_{\mathrm{ref}}$) results of KrakenC-Adiabatic(incoherent), Couple(coherent), Peregrine (coherent) and Eq.(19)(incoherent). The exact Rayleigh Reflection coefficient is used for Eq.(19). The source depth is 30 m. The squared sound pressure is averaged over receiver depths with 1 m resolution.

The differences between the baseline solution and adiabatic model solutions are summarized in the Table 2.

Table 2. Summary of multimodel comparisons for range dependent cases *(magnitude of difference, in dB)*.

	Method	250 Hz	1 kHz	3.5 kHz
		Maximum difference between baseline solution and adiabatic models	Maximum difference between baseline solution and adiabatic models	Maximum difference between baseline solution and adiabatic models
Case 4	KrakenC	0.35 dB	2.3 dB	n/a
	Eq.(19)	0.25 dB	2.2 dB	n/a
Case 9	KrakenC	0.6 dB	0.2 dB	0.4 dB
	Eq.(19)	0.4 dB	0.3 dB	0.6 dB

A final comparison is made between KrakenC and Eq.(19) to test the accuracy of the approximations made by Eq (19), as summarized in Table 3.

Table 3. Maximum difference between KrakenC and Eq.(19) *(magnitude of difference, in dB).*

	250 Hz	**1 kHz**	**3.5 kHz**
Case 1	0.1 dB	0.1 dB	0.1 dB
Case 4	0.1 dB	0.1 dB	0.2 dB
Case 9	0.1 dB	0.1 dB	0.1 dB

These comparisons and tables give an insight into the maximum average error of Eq.(19) for the three selected test cases.

2.3.5. SUMMARY AND CONCLUSIONS

In this section, practical approaches (Eq.(11) ,Eq.(13) and Eq.(19)) to calculate the propagation loss (PL) in range dependent waveguides are introduced. Eq.(11) is an analytical solution based on linear variation of reflection loss with angle. For long ranges, Eq.(11) asymptotically approaches to Eq.(13), which can be implemented without requiring a costly search for complex eigenvalues. Eq.(19) is a general form of solution which can be evaluated numerically by using the exact form of the Rayleigh reflection coefficient. The solutions based on Eq.(19) and exact Rayleigh reflection coefficient can take into account the leaky mode region. For selected test cases from the Weston Memorial Workshop, Eq.(19) achieves a similar accuracy to the adiabatic mode theory results (KrakenC) and is orders of magnitude faster at high frequency. The comparison with KrakenC results shows that Eq.(19) reproduces the depth and range dependent properties of incoherent mode theory without requiring long computational times.

The accuracy of adiabatic mode theory is investigated for selected test cases. PL is calculated with the propagation models KrakenC (adiabatic modes), Couple (coupled modes with single scatter option) and Peregrine (parabolic equation). The performance of each model for the selected test cases is tested.

For the range independent waveguide scenario (Case 1), the depth-averaged PL results of these models are very similar (the maximum diference is less than 0.15 dB). Given the entirely different nature of these methods[Ainslie,2010a], we interpret this difference as evidence that all models are providing the correct solution to Case 1, with an uncertainty of ± 0.15 dB.

For the range dependent cases (Case 4 and 9), the performance of the each algorithm is different. Eq.(19) replicates KrakenC (adiabatic mode theory) results to within 0.2 dB without requiring long computational times. However, the agreement between Couple and Peregrine and disagreement between Couple and KrakenC show the adiabatic approximation is not valid for Case 4 at 1 kHz after 19 km. The difference between Eq.(19) and the baseline solution is less than 0.6 dB for the selected test cases except 1 kHz result of Case 4.

APPENDIX A. EFFECTIVE DEPTH CONCEPT FOR THE RANGE DEPENDENT WAVEGUIDES

This section shows analytical implementation of the effective depth solution. The effective water depth is defined as[Weston,1976]

$$h_{\text{eff}} = \frac{h^2(0)h^2(r)}{r}\int_0^r \frac{1}{h^3(r')}\,\mathrm{d}r' \qquad (A1)$$

where $h(0)$ and $h(r)$ are the water depths at source and receiver ranges. An arbitrary depth profile can be separated into smaller segments as shown in Fig. A.1

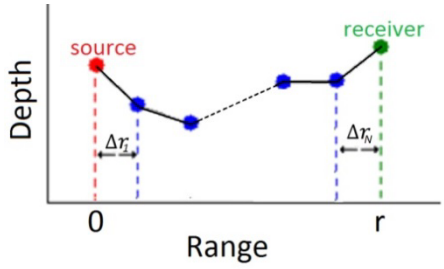

Figure A.1. Piecewise linear representation of bathymetry

where Δr_j is the horizontal length of *j*th segment as shown in Fig. A.1. Each segment can have different length. An analytical solution can be obtained by solving and summing the integrals for each segment. Weston's solution[Weston,1976] for upslope or downslope bathymetry can be generalized for arbitrary set of piecewise linear segments as

$$h_{\text{eff}} = \frac{h^2(0)h^2(r)}{r}\sum_{j=1}^{N}\Delta r_j \frac{h_j + h_{j+1}}{2\left(h_j h_{j+1}\right)^2} \qquad (A4)$$

where h_j is the water depth at the end of *j*th segment, Δr_j is the length of *j*th segment and *N* is the number of segments. In our calculation, a uniform segment length $\Delta r_j = \Delta r$ is used. For a range dependent sediment type, the integral can be evaluated as

$$\left\langle \frac{\eta}{h^3} \right\rangle = \frac{1}{r}\int_0^r \frac{\eta(r')}{h^3(r')}\mathrm{d}r' = \frac{1}{r}\left(\int_0^{\Delta r} \frac{\eta_1}{h^3}\mathrm{d}r' + \int_{\Delta r}^{2\Delta r} \frac{\eta_2}{h^3}\mathrm{d}r' + \cdots + \int_{(N-1)\Delta r}^{N\Delta r} \frac{\eta_N}{h^3}\mathrm{d}r'\right)$$
$$= \frac{1}{r}\sum_{j=1}^{N} \eta_j \Delta r_j \frac{h_j + h_{j+1}}{2\left(h_j h_{j+1}\right)^2} \qquad (A5)$$

where η is assumed constant for each segment. [Holland,2010] has derived a similar equation to solve range dependent sediment problems. Specifically, Eq. (A5) above is closely related to Holland's Eq. (4), which can be written $\left|\hat{R}\right| = \exp\left(-h^2(0)\theta_0^2 \left\langle \frac{\eta}{h^3} \right\rangle \frac{\tilde{r_c}}{2}\right)$ for isovelocity water. Where $\tilde{r_c}$ corresponds to weighted cycle distance (see Eq.(5) of Reference 6) and $\left|\hat{R}\right|$ is the geometric mean of the range dependent reflection coefficient.